Journal of Food Measurement and Characterization
https://doi.org/10.1007/s11694-024-02561-3

ORIGINAL PAPER

Multifunctional trimetal-organic frameworks with enhanced fenton-like catalytic activity for inhibiting bacteria

Hongbin Pu[1,2,3] · Qihong Ouyang[1,2,3] · Xiyi Zhou[1,2,3] · Da-Wen Sun[1,2,3,4]

Received: 11 October 2023 / Accepted: 12 April 2024

Abstract
Antibiotics and chemical disinfectants usually have serious problems of drug resistance and biosafety. Metal-organic frameworks (MOFs), as a new alternative method, have been studied to inhibit bacteria attributed to their tunability of compositions and structures, ideal biocompatibility and great catalytic properties. In the current study, two trimetal-organic frameworks ($Ni_1Co_1Fe_1$-MOFs and $Ni_6Co_3Fe_1$-MOFs) with different atomic ratios of Ni/Co/Fe were synthesized by a simple one-pot room temperature method. The fabricated MOFs showed outstanding Fenton-like catalytic activities and $Ni_1Co_1Fe_1$-MOFs exerted greater catalytic activity. Based on a Fenton-like reaction, a high-efficiency antibacterial system was constructed. The manufactured $Ni_1Co_1Fe_1$-MOF/sodium alginate composite coating delayed the weight loss of apple chunks and effectively inhibited *E. coli* bacteria from polluted apple chunks after storage for 2 d, significantly improving the fruit storage. This study proposed a novel and effective antibacterial strategy, which would open up a promising idea for the exploitation of food antibacterial agents in the future.

Keywords Metal-organic frameworks · Fenton-like catalytic activity · Antibacterial agent · *S. Aureus* · *E. Coli*

Introduction

Pathogenic bacteria widely exist in the environment and food [1, 2], inducing bacterial infectious disease with difficult recovery [3, 4] and high mortality[5, 6], which becomes the greatest public health concern [7, 8]. Traditional antibacterial agents, such as antibiotics [9] and chemical disinfectants [10], usually have problems with drug resistance and biosafety [11], thus it is needed to develop novel antibacterial agents [12].

With the developments of nanoscience [13, 14] and nanotechnology [15, 16], a variety of nano antibacterial agents have been constructed in recent years, including nanosilver [17], metal ions [18], metal/metal oxides [19], antibacterial peptides [20] and carbon nanomaterials [21], which have been employed to overcome the weaknesses of traditional antibacterial agents [22, 23]. Metal-organic frameworks (MOFs), as a novel porous nanomaterial, show great antibacterial activities [24]. The mechanisms of their antibacterial action are entirely different to those of antibiotics [25], thus such antibacterial materials provide a new alternative to conventional antibacterial strategies and can possibly solve the problem of drug resistance.

MOFs are constructed by metal ions or clusters and organic ligands that are connected by metal coordination, hydrogen bonding, electrostatic and π-π interaction [26, 27], generally possessing unique characteristics of high surface area [28], tunable porosity [29], flexible tailorability [30] and diversity in metal centres [31]. Based on these features, MOFs have been vastly investigated for a varying range of

✉ Da-Wen Sun
dawen.sun@ucd.ie
http://www.ucd.ie; http://www.ucd.ie/sun

1 School of Food Science and Engineering, South China University of Technology, Guangzhou 510641, China

2 Academy of Contemporary Food Engineering, South China University of Technology, Guangzhou Higher Education Mega Center, Guangzhou 510006, China

3 Engineering and Technological Research Centre of Guangdong Province on Intelligent Sensing and Process Control of Cold Chain Foods, & Guangdong Province Engineering Laboratory for Intelligent Cold Chain Logistics Equipment for Agricultural Products, Guangzhou Higher Education Mega Centre, Guangzhou 510006, China

4 Food Refrigeration and Computerized Food Technology (FRCFT), Agriculture and Food Science Centre, University College Dublin, National University of Ireland, Belfield, Dublin 4, Ireland

Published online: 15 May 2024

applications involving adsorption [32], gas sorption and separation [33], proton conductivity [34], sensors [35], biomedicine [36] and heterogeneous catalysis [37]. Similarly, MOFs also perform great potential in the antibacterial field [38, 39], mainly due to the well-dispersed metal active centres, in which the released metal cations can penetrate the membrane of bacterial cells, breaking the polarization state and the permeability of the membrane [40]. Therefore, benefiting from various metal nodes and a large number of optional organic linkers, the properties of MOFs can be modified and improved to achieve targeted functionality by adjusting the compositions and structures.

Hydrogen peroxide (H_2O_2), as an effective antibacterial agent, has been extensively applied in the practical treatment of bacterial infections [41], and hydroxyl radical (•OH) as the most toxic active substance shows stronger antibacterial activity than H_2O_2 and has attracted great research interests [42, 43]. Fenton-like reaction refers to the conversion of H_2O_2 to strongly oxidizing •OH by using transition metal ions, including Fe^{2+} [44], Ni^{2+} [45], Co^{2+} [46], Cu^{2+} [47], Mn^{2+} [48] and the like, as catalysts and is one of the most important sources of •OH. Therefore, the antibacterial performance of the antibacterial system can be effectively enhanced by introducing a Fenton-like reaction into it. The antibacterial principle is that the produced •OH can cause initial oxidative damage to bacterial cell membrane and increase membrane permeability, making it more sensitive to environmental conditions [49].

Interestingly, MOFs have been testified to play an important role in Fenton-like catalysts on account of highly dispersed metal sites and a mass of vacancies [50]. For example, Chen et al. [51] reported NH_2-Fe-MILs used for imidacloprid degradation as an outstanding Fenton-like catalyst, while Feng et al. [52] successfully fabricated bromine-functionalized bimetallic MOFs-FeCu (BDC-Br) to improve Fenton-like catalytic performance in water/wastewater treatment [53, 54] via increasing the interfacial electron transfer and reducing the electron density of bimetallic MOFs. However, to the best of our knowledge, there is only one article on the application of trimetal-organic frameworks as Fenton-like catalysts in the clinical antimicrobial therapy field [55], and applications of trimetal-organic frameworks as Fenton-like catalysts in the food antibacterial and preservation field has not yet been explored. Consequently, it is of great significance to develop trimetal-organic frameworks as Fenton-like catalysts for food antibacterial preservation.

Therefore, in the current work, two kinds of NiCoFe-MOFs ($Ni_1Co_1Fe_1$-MOFs and $Ni_6Co_3Fe_1$-MOFs) were designed with different atomic ratios of Ni/Co/Fe by adjusting the content of the metal precursors using a simple one-pot room temperature method. The NiCoFe-MOFs provided a variety of metal active centres and relatively large contact areas. Based on the abundant active catalytic sites, the Fenton-like catalytic activities of the as-prepared $Ni_1Co_1Fe_1$-MOFs and $Ni_6Co_3Fe_1$-MOFs were investigated using the Fenton indicator methylene blue (MB) in the presence of H_2O_2. Then, isopropyl alcohol (IPA) was used as a free radical scavenger to identify •OH generated from the oxidation of H_2O_2 upon the addition of the NiCoFe-MOFs. By utilizing the catalytic activity of NiCoFe-MOFs, an antibacterial system based on a Fenton-like reaction was constructed against both gram-positive (*S. aureus*) and gram-negative (*E. coli*) bacteria, aiming to enhance the antibacterial property of the system via the generation of •OH and obtain broad-spectrum antibacterial activities. Moreover, the biocompatibility of both $Ni_1Co_1Fe_1$-MOFs and $Ni_6Co_3Fe_1$-MOFs was studied. Finally, the application of $Ni_1Co_1Fe_1$-MOFs/sodium alginate composite coating in food antibacterial preservation using apple as a model fruit was explored.

Materials and methods

Materials and reagents

Cobalt (II) acetate tetrahydrate ($Co(CH_3COO)_2{\cdot}4H_2O$), ferrous acetate tetrahydrate ($Fe(CH_3COO)_2{\cdot}4H_2O$), 2-amino terephthalic acid (H_2-$BDCNH_2$), MB, acetic acid (HAc), sodium hydroxide (NaOH), sodium chloride (NaCl) and glutaraldehyde were obtained from Shanghai Macklin Biochemical Co., Ltd. (Shanghai, China). Nickel (II) acetate tetrahydrate ($Ni(CH_3COO)_2{\cdot}4H_2O$), N, N′-dimethylformamide (DMF), sodium acetate anhydrous (NaAc), isopropyl alcohol and 2′,7′-dichlorodihydrofluorescein diacetate (DCFH-DA) were purchased from Aladdin Reagent Co., Ltd. (Shanghai, China). Hydrogen peroxide (H_2O_2, 30%) was supplied by Chengdu Chron Chemicals Co., Ltd. (Chengdu, China). Ethanol was bought from Guangdong Guanghua Sci-Tech Co., Ltd. (Guangdong, China). Hydrochloric acid (HCl) was acquired from Guangzhou Chemical Reagent Factory Co., Ltd. (Guangzhou, China). Propidium iodide (PI) was obtained from Beijing Solarbio Science & Technology Co., Ltd. (Beijing, China). SYTO 9 was supplied by Thermo Fisher Scientific Co., Ltd. (Waltham, USA). Dulbecco's modified eagle medium (DMEM), fetal bovine serum and PBS powder ($1\times$) were purchased from Sangon Biotech Co., Ltd. (Shanghai, China). Luria-Bertani (LB) broth and LB agar were obtained from Huankai Microbial Co., Ltd. (Guangdong, China). Penicillin-streptomycin and CCK-8 kit were obtained from Biyuntian Biotechnology Co., Ltd. (Shanghai, China). *Staphylococcus aureus* (*S. aureus*, ATCC-6538), *Escherichia coli* (*E. coli*, ATCC-700,728) and mouse 3T3 fibroblasts were acquired from ATCC (Manassas, Virginia, USA). Sodium alginate, ascorbic acid and

citric acid were acquired from Qiangli Chemical Products Co., Ltd. (Henan, China). Calcium chloride was obtained from Dacheng Calcium Industry Co., Ltd. (Zhejiang, China). Glycerol was purchased from Procter & Gamble Co. (USA). Peptone was supplied by Aoboxing Biotechnology Co., Ltd. (Beijing, China). Fresh apples were bought from a local market (Guangzhou, China). Deionized water (18.2 MΩ cm, Millipore) was used throughout this study.

Synthesis of NiCoFe-MOFs

The trimetallic NiCoFe-based MOFs were synthesized by the simple one-pot solution-phase method at room temperature of 25 °C as illustrated in Scheme 1A [55]. Firstly, 0.3333 mmol of $Ni(CH_3COO)_2{\cdot}4H_2O$ (82.9 mg), 0.3333 mmol of $Co(CH_3COO)_2{\cdot}4H_2O$ (83 mg) and 0.3333 mmol of $Fe(CH_3COO)_2{\cdot}4H_2O$ (82 mg) were dissolved into 10 mL of DMF (Solution A) and 1 mmol of H_2-$BDCNH_2$ (181.1 mg) was dissolved with 5 mL of DMF (Solution B), respectively. Then, Solution A and Solution B were quickly mixed and stirred by using a magnetic stirrer (85–2, Changzhou Putian Instrument and Equipment Industry Co., Ltd., Changzhou, China) for 1 h at a room temperature of 25 °C. The mixture solution was centrifuged by a centrifuge (JW-3024 h, Anhui Jiawen Instrument and Equipment Industry Co., Ltd., Hefei, China) and washed with DMF and ethanol several times. Finally, the $Ni_1Co_1Fe_1$-MOFs product was obtained by vacuum-drying using a vacuum-drying oven (DZF-6050, Shanghai Qixin Scientific Instrument Co., Ltd., Shanghai, China) at 60 °C for 12 h. The synthesis procedure of $Ni_6Co_3Fe_1$-MOFs was identical through adjusting the molar ratio of the used $Ni(CH_3COO)_2{\cdot}4H_2O$, $Co(CH_3COO)_2{\cdot}4H_2O$ and $Fe(CH_3COO)_2{\cdot}4H_2O$. To compare the properties of as-prepared NiCoFe-MOFs ($Ni_1Co_1Fe_1$-MOFs or $Ni_6Co_3Fe_1$-MOFs) with M-MOFs (M = Ni, Co, Fe), the Ni-MOFs, Co-MOFs and Fe-MOFs were synthesized by the same method as above.

Characterization of MOFs

The structure and morphology of the prepared MOFs were characterized by high-resolution field emission scanning electron microscopy (SEM, Merlin, Carl Zeiss AG, Oberkochen, Germany) and transmission electron

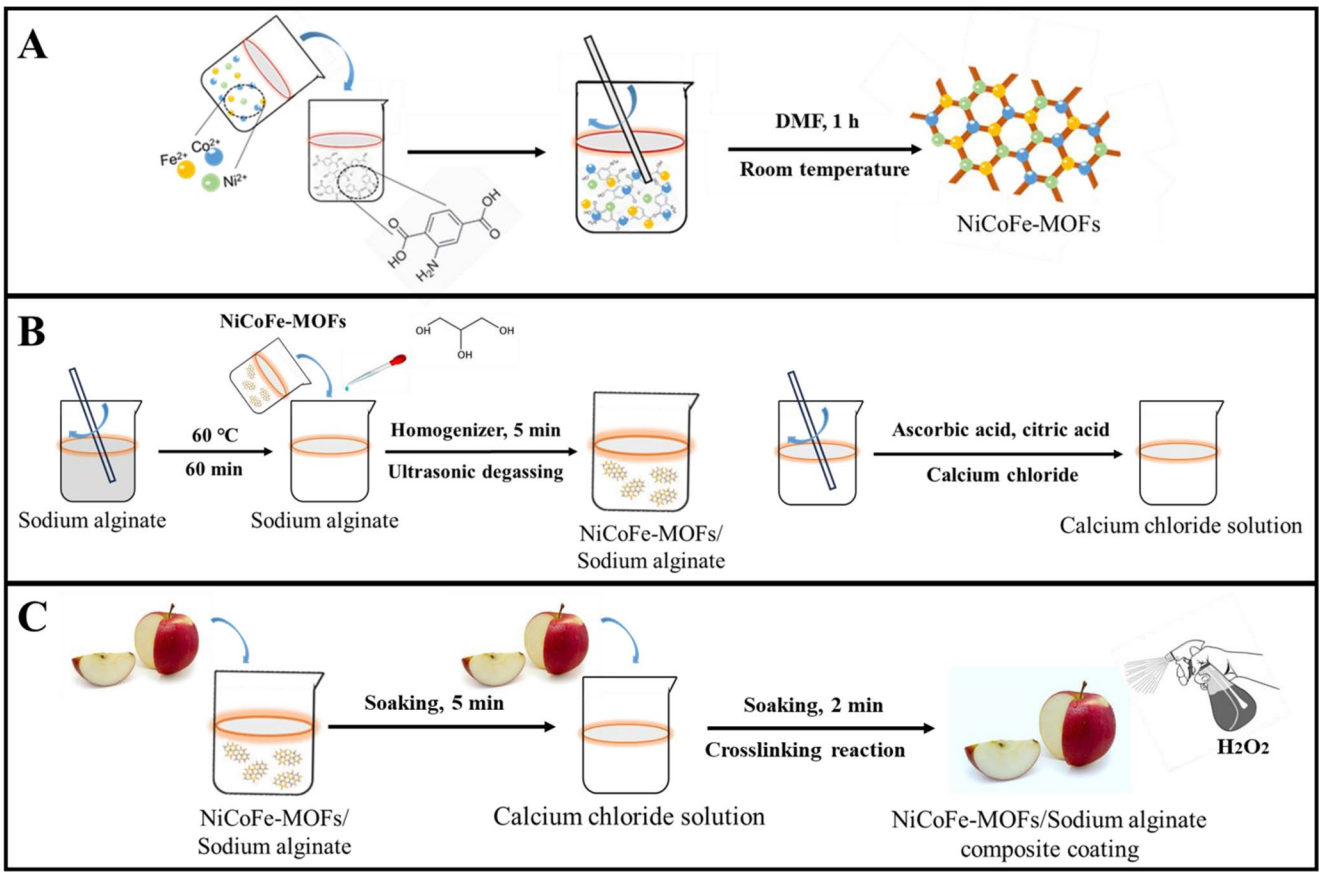

Scheme 1 (**A**) The synthesis process of NiCoFe-MOFs. (**B**) The preparation process of NiCoFe-MOF/sodium alginate mixed solution and calcium chloride solution. (**C**) The fabrication process of NiCoFe-MOF/sodium alginate complex coating and NiCoFe-MOF/sodium alginate composite coating + H_2O_2 on the surface of apple chunks

microscopy (TEM, JEM-1400 Plus, JEOL Ltd., Tokyo, Japan). The element mapping images were taken from high-angle annular dark-field scanning transmission electron microscopy (HAADF-STEM, FEI Talos F200X, Thermo Fisher Scientific Inc., Oregon, USA) and energy-dispersive X-ray spectroscopy (EDS, Axis Ultra DLD, Kratos Co., Manchester, UK). The chemical images were observed by Fourier-transform infrared spectroscopy (FT-IR, Thermo-Nicolet Co., Waltham, USA) and X-ray photoelectron spectroscopy (XPS, Kratos Analytical Ltd., Manchester, UK).

Characterization of fenton-like catalytic activity

To monitor the Fenton-like catalytic property of $Ni_1Co_1Fe_1$-MOFs and $Ni_6Co_3Fe_1$-MOFs, an MB molecular probe was used and experiments were carried out in HAc-NaAc buffer solution (0.2 M, pH 4.0). Briefly, different concentrations of $Ni_1Co_1Fe_1$-MOFs or $Ni_6Co_3Fe_1$-MOFs and different concentrations of H_2O_2 were separately added into the MB solution (0.1 mM) to build a redox reaction for 1 h at 37 °C. Then, the reaction mixture was centrifuged to remove the MOFs and the absorbance value of the supernatant at 664 nm was measured by a microplate reader (Synergy2, BioTek Instruments, Inc., Winooski, VT, USA).

Measurement of •OH

IPA was utilized as a quenching agent of free radicals. IPA could react with •OH to inhibit the degradation of MB [56] and experiments were carried out in HAc-NaAc buffer solution (0.2 M, pH 4.0). In detail, 200 μL aqueous solution containing MB (0.1 mM), $Ni_1Co_1Fe_1$-MOFs or $Ni_6Co_3Fe_1$-MOFs (200 μg/mL), H_2O_2 (20 mM) and a series of IPA concentrations (0, 10, 25, 50, 100 mM) were incubated at 37 °C. Then, the absorbance value of the supernatant at 664 nm was monitored by a microplate reader every 15 min.

In vitro antibacterial experiment

An agar plate counting method was used to evaluate the in vitro antibacterial efficiency of NiCoFe-MOFs ($Ni_1Co_1Fe_1$-MOFs or $Ni_6Co_3Fe_1$-MOFs). Gram-positive *Staphylococcus aureus* (*S. aureus*, ATCC 6538) and gram-negative *Escherichia coli* (*E. coli*, ATCC 700,728) were chosen as model bacteria [57]. LB broth was employed as culture media. After reaching the logarithmic period, the bacterial dispersion was diluted with a phosphate-buffered solution (PBS, pH 7.2) to 10^6 CFU/mL. Then, 4.5 mL of the prepared bacterial suspension was mixed with 0.5 mL of PBS, H_2O_2, NiCoFe-MOFs ($Ni_1Co_1Fe_1$-MOFs or $Ni_6Co_3Fe_1$-MOFs) and NiCoFe-MOFs + H_2O_2 for 2 h at 37 °C. The final concentrations of NiCoFe-MOFs and H_2O_2 were 100 μg/mL and 0.1 mM, respectively. Finally, the treated bacterial solution was spread and cultured on agar plates at 37 °C for 18 h before CFU enumeration.

For lived/dead bacterial analysis, both *S. aureus* and *E. coli* of the above treatment groups were harvested via centrifugation and washed twice. The obtained bacteria were stained with propidium iodide (PI, 10 μM) and SYTO 9 (10 μM) in the dark for 30 min. The dead bacteria were stained red fluorescence by PI and the live bacteria were stained green fluorescence by SYTO 9. Then, all samples were centrifuged, washed with PBS, and imaged through a laser scanning confocal microscope (TCS SP8, Leica Microsystems GmbH, Wetzlar, Germany).

To evaluate the antibacterial effects under different treatment protocols, the morphology of bacteria was observed by SEM. After treatment, the bacteria were collected by centrifugation and washed twice with PBS. Then the obtained bacteria were fixed with 2.5% glutaraldehyde solution overnight at 4 °C. After washing with PBS three times, they were dehydrated by graded ethanol solutions (30%, 50%, 70%, 80, 90% and 100%). Next, the samples were dried at room temperature in the vacuum drying oven. After drying, they were sputter-coated with platinum for SEM observation.

Measurement of intracellular ROS

The oxidant-sensitive dye 2′,7′-dichloro-dihydro-fluorescein (DCFH-DA), as a fluorescent probe, was utilized to test intracellular ROS levels. After reaching the logarithmic period, the diluted bacterial suspension (10^6 CFU/mL) was incubated with DCFH-DA (20 μM) at 37 °C for 30 min in the dark. The bacteria were then collected by centrifugation, washed with PBS, and treated with PBS, H_2O_2, $Ni_1Co_1Fe_1$-MOFs and $Ni_1Co_1Fe_1$-MOFs + H_2O_2 for 2 h at 37 °C. The final concentrations of NiCoFe-MOFs and H_2O_2 were 100 μg/mL and 0.1 mM, respectively. Intracellular ROS were estimated via the microplate reader with excitation wavelength at 488 nm and emission at 525 nm.

Cytotoxicity assay

Mouse embryonic fibroblast (NIH-3T3) cells were employed for in vitro cytotoxicity study of NiCoFe-MOFs ($Ni_1Co_1Fe_1$-MOFs or $Ni_6Co_3Fe_1$-MOFs). NIH-3T3 cells at a density of 5×10^3 cells per well were seeded in a 96-well plate and cultured in a DMEM medium containing 10% fetal bovine serum and 1% penicillin-streptomycin. After maintaining 24 h in 5% CO_2 at 37 °C, the culture media was discarded, and NIH-3T3 cells were washed with PBS. The obtained cells were treated with H_2O_2, NiCoFe-MOFs ($Ni_1Co_1Fe_1$-MOFs or $Ni_6Co_3Fe_1$-MOFs) and NiCoFe-MOFs + H_2O_2 for 24 h. The cells without NiCoFe-MOFs

and H_2O_2 were applied as a control. After washing with PBS, the cell viability of NIH-3T3 was determined via a cell counting kit-8 (CCK-8, Biyuntian Biotechnology Co., Ltd., Shanghai, China). Moreover, the cytotoxicity study of NiCoFe-MOFs at different concentrations (12.5, 25, 50, 100 and 200 μg/ mL) was also performed, and the cells without NiCoFe-MOFs were applied as a control.

Fruit storage experiments

To explore the antibacterial and preservation effects of the NiCoFe-MOFs/sodium alginate complex coating, $Ni_1Co_1Fe_1$-MOF was chosen as an antibacterial agent. Apple was selected as a model fruit [58]. Gram-negative Escherichia coli (*E. coli*, ATCC 700,728) was employed as a model bacterium [59].

For obtaining $Ni_1Co_1Fe_1$-MOF/sodium alginate mixed solution, at first, 1.5 g of sodium alginate was dissolved in 100 mL of water, and the solution was stirred for 60 min in a water bath at 60 °C (MS7-H550-Pro, DLAB Scientific Co., Ltd., Beijing, China) until the solution became clear and transparent. Then, 1.5 g of glycerol and 10 mg of $Ni_1Co_1Fe_1$-MOF were introduced into the sodium alginate solution and the $Ni_1Co_1Fe_1$-MOF/sodium alginate mixed solution was mixed by a homogenizer for 5 min (QIQIAN-08, Qiqian Electronic Technology Co., Ltd., Shanghai, China). After homogenizing, the $Ni_1Co_1Fe_1$-MOF/sodium alginate mixed solution was degassed with ultrasonic (SB25-12D, Ningbo Xinyi Ultrasonic Equipment Co., Ltd., Zhejiang, China). In addition, a calcium chloride solution was acquired by dissolving 10 g of calcium chloride, 5 g of ascorbic acid and 5 g of citric acid in 500 mL of water as illustrated in Scheme 1B.

Fresh apples were cleaned with tap water, sterile water, and 75% alcohol in sequence. Clean apples were cored and cut into 10 g of small pieces. LB broth was employed as culture media of *E. coli*. After reaching the logarithmic period, the *E. coli* dispersion was diluted with 0.1% (w/v) of peptone solution to 10^6~10^7 CFU/mL. Then, 500 μL of the prepared *E. coli* suspension was inoculated on a small piece of apple. After inoculation, polluted apple chunks were air dried for 60 min in a microbial ultra-clean workbench (BCL-1800 A/B, Yatai Kelon Instrument Co., Ltd., Beijing, China).

The polluted apple chunks were divided into three groups, including uncoated control, coated with $Ni_1Co_1Fe_1$-MOF/sodium alginate or $Ni_1Co_1Fe_1$-MOF/sodium alginate + H_2O_2. The $Ni_1Co_1Fe_1$-MOF/sodium alginate composite coating was performed by soaking the polluted apple chunks in $Ni_1Co_1Fe_1$-MOF/sodium alginate mixed solution for 5 min and then soaking them in calcium chloride solution for 2 min, based on the cross-linking reaction between sodium alginate and calcium chloride. After coating, polluted apple chunks were air dried for 60 min in a microbial ultra-clean workbench. The group of NiCoFe-MOFs/sodium alginate + H_2O_2 was acquired by spraying the coated and polluted apple chunk surface with a small amount of H_2O_2 as illustrated in Scheme 1C. The apple samples were then stored for 10 d in a refrigerator at 4 °C (BCD-539WT, Qingdao Haier Co., Ltd., Shandong, China). The weight losses and antibacterial effect of the apple samples were recorded on days 0, 2, 4, 6, 8 and 10. For antibacterial effect analysis, apple samples after storage were mixed with 90 mL 0.1% (w/v) of peptone solution and homogenized for 2 min at 8 times/s. Finally, the supernatant fluid was spread and cultured on agar plates at 37 °C for 18 h before CFU enumeration.

Statistical analysis

All experiments were conducted in triplicate except otherwise stated and results were expressed as means ± standard deviation. One-way analysis of variance (ANOVA) was utilized using Office Excel 2019 (Microsoft Corp., Redmond, USA) to determine the differences between groups, with significances given at * $p < 0.05$, ** $p < 0.01$, and *** $p < 0.001$.

Results and discussion

Synthesis and characterization of NiCoFe-MOFs

The morphologies and structures of $Ni_1Co_1Fe_1$-MOFs and $Ni_6Co_3Fe_1$-MOFs were first examined by SEM as shown in Fig. 1A-B and E-F, respectively. The results showed that the as-prepared $Ni_1Co_1Fe_1$-MOFs exhibited a 3D foam-like architecture comprising interconnected nanofibers, and $Ni_6Co_3Fe_1$-MOFs exhibited a nanoflower-like architecture with uniform size and good dispersion. The SEM results were verified by TEM images (Fig. 1C, G), where $Ni_6Co_3Fe_1$-MOFs showed uniform nanoflowers with a diameter of about 2 μm. The HAADF-STEM images and EDS elemental mapping results (Fig. 1D, H) indicated that C, N, O, Ni, Co and Fe elements existed and were uniformly distributed throughout the whole microstructures of $Ni_1Co_1Fe_1$-MOFs and $Ni_6Co_3Fe_1$-MOFs, respectively. In addition, to confirm the formation of MOF structure, the FT-IR spectra (Fig. 1I) were further collected, showing significantly similar characteristic peaks of H_2-BDCNH$_2$ and MOFs. The absorption peaks at 752 cm^{-1}, 1230 cm^{-1}, 1420 cm^{-1} and 3390 cm^{-1} could be attributed to the bending vibrations of C-H on the benzene rings, and the stretching vibrations of the C-N, C = O and O-H, respectively. The peaks at 494 cm^{-1} and

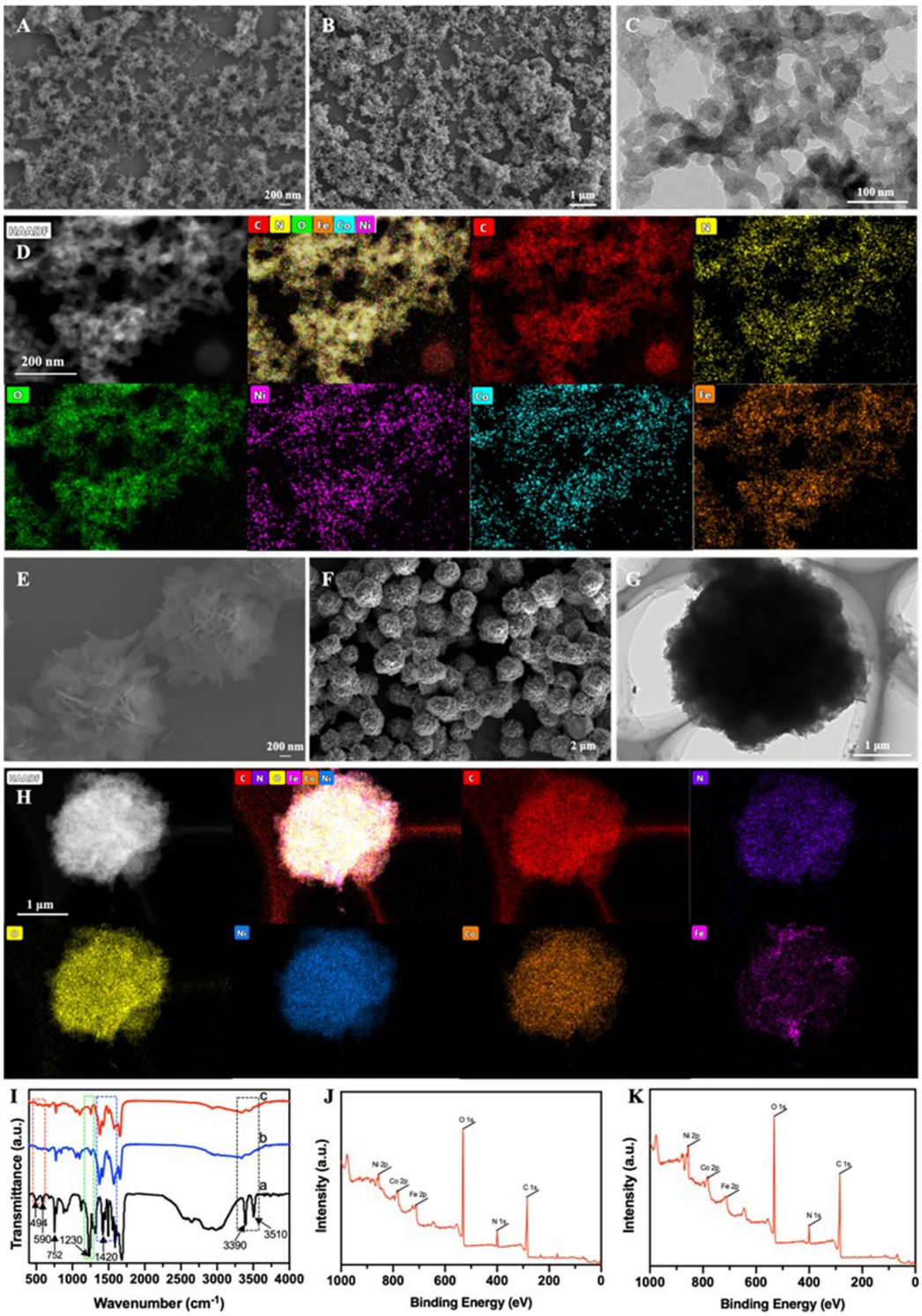

Fig. 1 (**A**-**B**) SEM and (**C**) TEM images of $Ni_1Co_1Fe_1$-MOFs, (**D**) HAADF-STEM image and corresponding EDS elemental mapping analysis of $Ni_1Co_1Fe_1$-MOFs, (**E**-**F**) SEM and (**G**)TEM images of $Ni_6Co_3Fe_1$-MOFs, (**H**) HAADF-STEM image and corresponding EDS elemental mapping analysis of $Ni_6Co_3Fe_1$-MOFs, (**I**) FT-IR spectra of (a) H_2-$BDCNH_2$, (b) $Ni_6Co_3Fe_1$-MOFs and (c) $Ni_1Co_1Fe_1$-MOFs, (J) XPS survey of $Ni_1Co_1Fe_1$-MOFs, (**K**) XPS survey of $Ni_6Co_3Fe_1$-MOFs

590 cm^{-1} were due to the longitudinal and transverse vibration of Ni-O/Co-O/Fe-O, respectively [60, 61]. The characteristic peak at 3510 cm^{-1} belonged to the primary amine stretching vibrations of H_2-$BDCNH_2$ [62]. Compared with H_2-$BDCNH_2$, the peaks at 1420 cm^{-1} and 3390 cm^{-1} were both obviously weakened, while the peaks corresponding to symmetrical and asymmetric vibration of the carboxyl groups were found near at 1380 cm^{-1} and 1575 cm^{-1}, respectively, which could be assigned to the coordination between H_2-$BDCNH_2$ and metal ions. Besides, the significant reduction in the peak at 3510 cm^{-1} further manifested the coordination structure of NiCoFe-MOFs. The formation of $Ni_1Co_1Fe_1$-MOFs and $Ni_6Co_3Fe_1$-MOFs were further validated by XPS (Fig. 1J, K). Specifically, there were six elements of carbon (C1s, 285 eV), nitrogen (N1s, 400 eV), oxygen (O1s, 532 eV), nickel (Ni2p, 856 eV), cobalt (Co2p, 782 eV) and iron (Fe2p, 713 eV) in both $Ni_1Co_1Fe_1$-MOFs and $Ni_6Co_3Fe_1$-MOFs, which indicated the successful preparation of trimetal-organic frameworks.

Fenton-like catalytic activity of NiCoFe-MOFs

Based on the successful preparation of $Ni_1Co_1Fe_1$-MOFs and $Ni_6Co_3Fe_1$-MOFs, their Fenton-like catalytic activity was evaluated by the Fenton indicator MB in the presence of H_2O_2. As shown in Fig. 2A, $Ni_1Co_1Fe_1$-MOFs and $Ni_6Co_3Fe_1$-MOFs exhibited significant catalytic activity after adding H_2O_2 and MB, in which the catalytic activity of $Ni_1Co_1Fe_1$-MOFs was better. In contrast, the same amount of either MOFs or H_2O_2 alone could hardly cause MB degradation. Besides, in comparison with Ni-MOFs, Co-MOFs and Fe-MOFs, $Ni_1Co_1Fe_1$-MOFs had the highest Fenton-like catalytic efficiency (Fig. 2B), albeit $Ni_6Co_3Fe_1$-MOFs were more efficient than M-MOFs (M = Ni, Co, Fe). These phenomena manifested that $Ni_1Co_1Fe_1$-MOFs and $Ni_6Co_3Fe_1$-MOFs could effectively degrade MB by the generation of •OH in the presence of H_2O_2, and the introduction of Ni/Co/Fe effectively improved the Fenton-like catalytic performance of NiCoFe-MOFs, which was consistent with previous reports [31, 60]. Similar to most Fenton catalysts, the absorbance of MB was affected by MOF concentration, H_2O_2 concentration, incubation pH and incubation time (Fig. 2C-F). As shown in Fig. 2C, D, within a certain range of MOFs or H_2O_2 concentrations, the degradation rate of MB increased as the concentrations increased. When the MOFs or H_2O_2 concentrations continued to increase after reaching the optimal concentrations, the degradation rate of MB decreased gradually, which was due to that •OH would be quenched by excessive Fe^{2+} or H_2O_2, hindering the Fenton-like reaction [63]. Figure 2E shows that the catalytic efficiency of $Ni_1Co_1Fe_1$-MOFs and $Ni_6Co_3Fe_1$-MOFs achieved the maximum at pH 3.5, then decreased as pH increased. Subsequently, the time dependence of the catalytic reaction was further investigated (Fig. 2F). With the extension of time, the catalytic effect of MOFs was greatly enhanced in the presence of H_2O_2, in which $Ni_1Co_1Fe_1$-MOFs performed better, while MOFs or H_2O_2 alone had almost no catalytic activity, which further verified the above conclusions.

To determine the production of •OH as the main active substance in the Fenton-like system, IPA was used as a capture agent of free radicals to react with •OH, which could hinder the degradation of MB. As shown in Fig. 2G-H, after adding 10 mM IPA into the system, the degradation rate of MB was significantly inhibited and was further inhibited as the concentration of IPA increased. Thus, the results obviously demonstrated that the as-prepared $Ni_1Co_1Fe_1$-MOFs and $Ni_6Co_3Fe_1$-MOFs, as Fenton-like catalysts, could oxidize H_2O_2 to form •OH.

In vitro antibacterial test

Motivated by the excellent Fenton-like catalytic activity of $Ni_1Co_1Fe_1$-MOFs and $Ni_6Co_3Fe_1$-MOFs, their in vitro antibacterial abilities were evaluated against both gram-positive *S. aureus* and gram-negative *E. coli*. Primarily, the antibacterial property of H_2O_2 was investigated (Fig. 3A, B). H_2O_2 possesses effective antibacterial activity, which has been widely applied to treat bacterial infections. However, compared with H_2O_2, •OH can lead to more serious oxidative damage to bacteria. Consequently, the as-prepared $Ni_1Co_1Fe_1$-MOFs and $Ni_6Co_3Fe_1$-MOFs were expected to enhance the antibacterial efficiency of H_2O_2 and thus the antibacterial properties of H_2O_2 alone and H_2O_2 plus MOFs against *S. aureus* and *E. coli* were respectively tested. The results showed that the H_2O_2 concentration could be reduced by about one to two orders of magnitude in the presence of MOFs. Encouraged by these findings, the corresponding antibacterial abilities of $Ni_1Co_1Fe_1$-MOFs and $Ni_6Co_3Fe_1$-MOFs were further evaluated, and results are shown in Fig. 3C-D, indicating that $Ni_1Co_1Fe_1$-MOFs and $Ni_6Co_3Fe_1$-MOFs performed strong dose-dependent antibacterial efficiencies. $Ni_1Co_1Fe_1$-MOFs and $Ni_6Co_3Fe_1$-MOFs could almost achieve complete antibacterial effects at the concentration of MOFs of 100 μg/mL after adding H_2O_2. The time-dependent antibacterial efficiencies were also investigated as presented in Fig. 3E, F. Both $Ni_1Co_1Fe_1$-MOFs and $Ni_6Co_3Fe_1$-MOFs performed slightly antibacterial activities, while when 0.1 mM H_2O_2 were added, the MOFs could strongly inhibit *S. aureus* and *E. coli* with the best incubation time of 2 h. In particular, $Ni_1Co_1Fe_1$-MOFs exhibited more effective antibacterial activity than $Ni_6Co_3Fe_1$-MOFs, as $Ni_1Co_1Fe_1$-MOFs had stronger catalytic activity for the production of •OH.

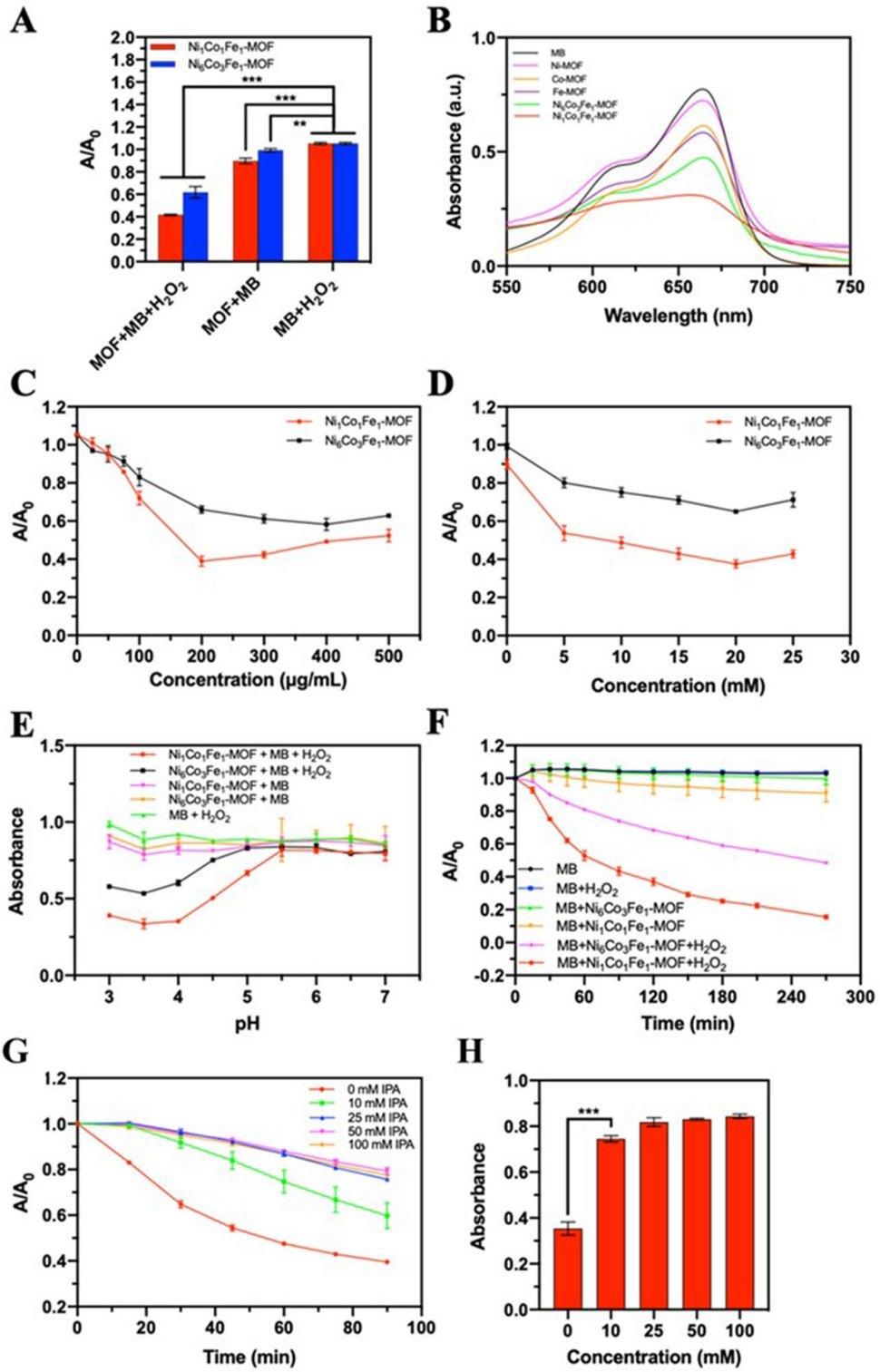

Fig. 2 Fenton-like catalytic activities of $Ni_1Co_1Fe_1$-MOFs and $Ni_6Co_3Fe_1$-MOFs. (**A**) Absorption of MB treated with H_2O_2, MOFs ($Ni_1Co_1Fe_1$-MOFs or $Ni_6Co_3Fe_1$-MOFs) and MOFs + H_2O_2 for 1 h, the final concentrations of MOFs and H_2O_2 were 200 μg/mL and 20 mM, respectively. Values are displayed as means ± s.d. ($n = 3$). *$P < 0.05$, **$P < 0.005$, ***$P < 0.001$. (**B**) UV-Vis absorption spectra of MB with different MOFs, (**C**) Absorption of MB treated with $Ni_1Co_1Fe_1$-MOFs or $Ni_6Co_3Fe_1$-MOFs at the concentration of 25, 50, 75, 100, 200, 300, 400, 500 μg/mL containing 20mM H_2O_2, (**D**) Absorption of MB treated with H_2O_2 at the concentration of 5, 10, 15, 20, 25 mM, containing 200 μg/mL MOFs ($Ni_1Co_1Fe_1$-MOFs or $Ni_6Co_3Fe_1$-MOFs), (**E**) Absorbance value of MB under different pH, containing 20mM H_2O_2 and 200 μg/mL MOFs ($Ni_1Co_1Fe_1$-MOFs or $Ni_6Co_3Fe_1$-MOFs), (**F**) Real-time absorption of MB in different reaction systems: (1) control, (2) H_2O_2, (3) MOFs ($Ni_1Co_1Fe_1$-MOFs or $Ni_6Co_3Fe_1$-MOFs) and (4) MOFs + H_2O_2, the final concentrations of MOFs and H_2O_2 were 200 μg/mL and 20 mM, respectively, (**G**) Time-dependent curves of MB absorption at different IPA concentrations, (**H**) Capture of •OH incubated with IPA at different concentrations for 1 h. Values are displayed as means ± s.d. ($n = 3$). *$P < 0.05$, **$P < 0.005$, ***$P < 0.001$

To further evaluate the synergistic antibacterial effect, 0.1 mM H_2O_2 and 100 μg/mL NiCoFe-MOFs ($Ni_1Co_1Fe_1$-MOFs or $Ni_6Co_3Fe_1$-MOFs) were employed. As shown in Fig. 4A-C, the control group showed 100% viable *S. aureus* and *E. coli* with a mass of colonies on LB agar plates. After treating with H_2O_2 and $Ni_1Co_1Fe_1$-MOFs alone, the viability of *S. aureus* and *E. coli* exhibited a slight decrease. A rational reason for this phenomenon was that a low concentration of H_2O_2 had a poor antibacterial effect and the release of Ni^{2+}, Co^{2+} and Fe^{2+} in $Ni_1Co_1Fe_1$-MOFs could act on bacterial cell membranes, causing the death of a few bacteria [40, 42]. Upon simultaneous treatment with H_2O_2 and

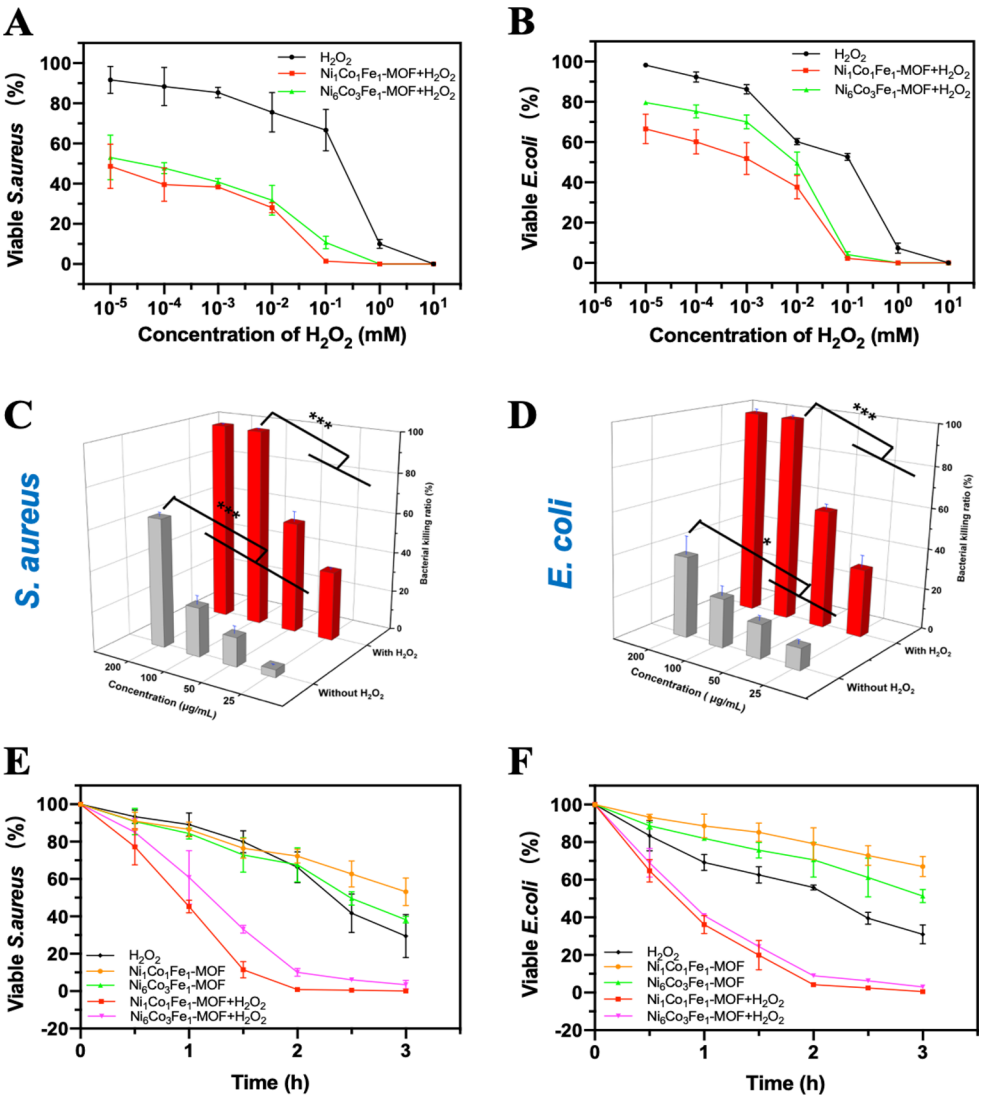

Fig. 3 Survival rates of (**A**) *S. aureus* and (**B**) *E. coli* treated with H_2O_2 at different concentrations with or without MOFs ($Ni_1Co_1Fe_1$-MOFs or $Ni_6Co_3Fe_1$-MOFs) for 2 h; Killing rates of (**C**) *S. aureus* and (**D**) *E. coli* treated with $Ni_1Co_1Fe_1$-MOFs at concentrations of 200, 100, 50, 25 μg/mL with or without H_2O_2. Values are displayed as means ± s.d. ($n = 3$). $^*P < 0.05$, $^{**}P < 0.005$, $^{***}P < 0.001$. Time-dependent survival rates of (**E**) *S. aureus* and (**F**) *E. coli* treated with (1) H_2O_2, (2) MOFs ($Ni_1Co_1Fe_1$-MOFs or $Ni_6Co_3Fe_1$-MOFs) and (3) MOFs + H_2O_2

$Ni_1Co_1Fe_1$-MOFs, the antibacterial rates of *S. aureus* and *E. coli* were increased remarkably to 99.17% and 98.10%, respectively, confirming that a Fenton-based synergetic antibacterial system was successfully established. A similar antibacterial tendency was observed in the treatment of $Ni_6Co_3Fe_1$-MOFs.

The integrity of the bacterial cell membrane was characterized by live/dead assays based on fluorescence. SYTO 9 stained the living bacteria with intact cell membranes green, and PI stained the dead bacteria with damaged membranes red. As shown in Fig. 4D, the intense green fluorescence of the bacteria was observed in the control group without red fluorescence, revealing that most bacteria were alive. In the H_2O_2 or MOFs treatment groups, only a few bacteria cells emitted red fluorescence, which corresponded to the results of agar plates counting above. Cotreatment of H_2O_2 and MOFs induced an apparent increase of the red spots, manifesting the Fenton-like reaction, dramatically boosting the antibacterial efficiency. All the results further affirmed the synergistically enhanced antibacterial property of H_2O_2 by $Ni_1Co_1Fe_1$-MOFs.

To further decipher the antibacterial effect, the changes in cell morphologies of *S. aureus* and *E. coli* were characterized by SEM, as presented in Fig. 4E. The untreated *S. aureus* (I) and *E. coli* (V) had an intact and smooth bacterial surface, in which the cells of *S. aureus* appeared as cocci and the cells of *E. coli* were typical bacillus. When the bacteria were exposed to H_2O_2 (II, VI) or MOFs (III, VII), the surface of bacterial cells turned slightly cupped and wrinkled, which demonstrated that H_2O_2 or MOFs alone had a minor effect on the membrane integrity of bacterial cells. Especially, the traversed pores were observed in the bacterial membranes, which might be due to that the released Ni^{2+}, Co^{2+} and Fe^{2+} ions would massively penetrate the bacteria cells and cause bacterial membrane defects [64]. Remarkably, in the MOFs + H_2O_2 treatment groups (IV, VIII), the

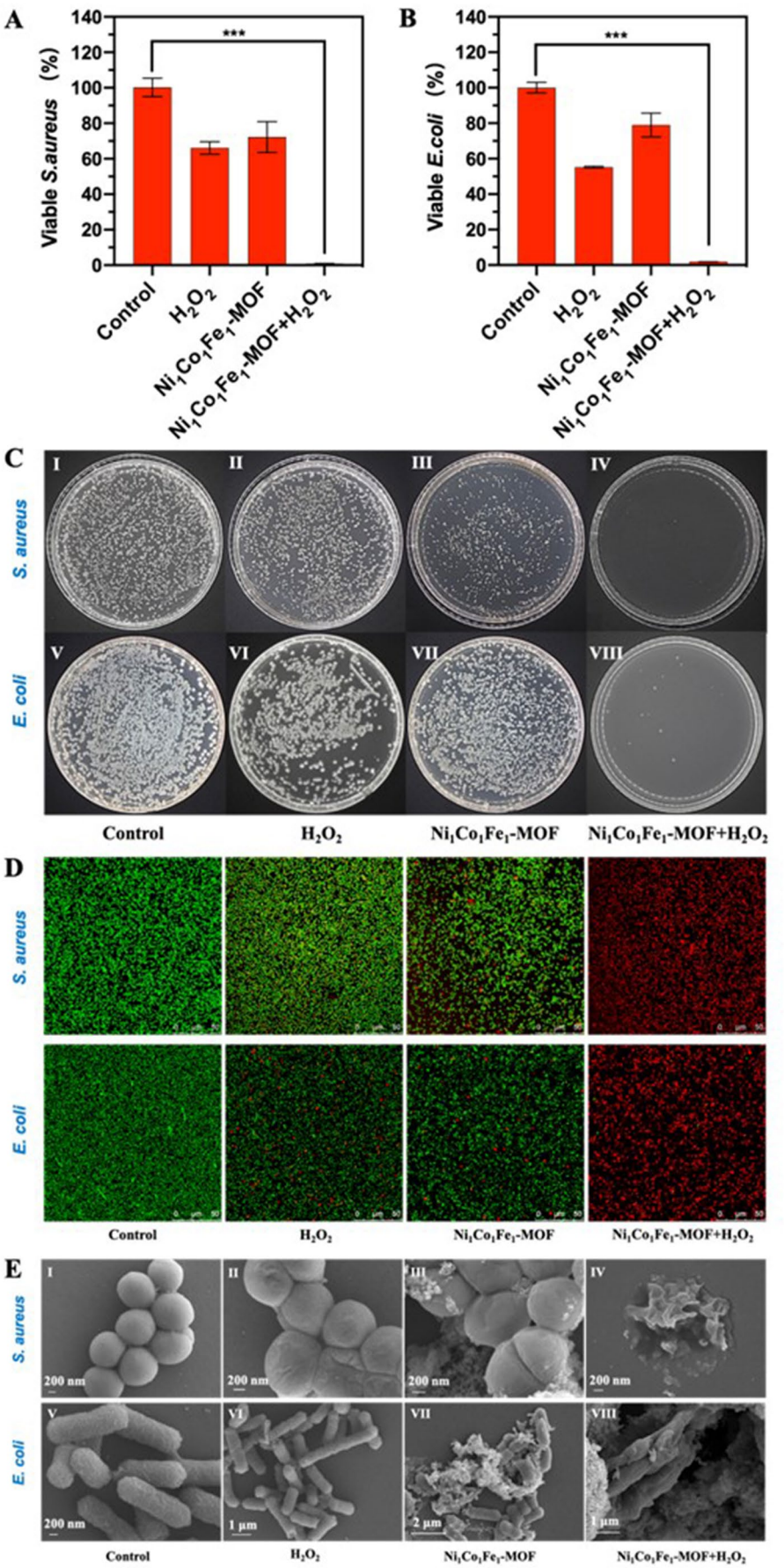

Fig. 4 Survival rates of (**A**) *S. aureus* and (**B**) *E. coli* treated with (1) PBS, (2) H_2O_2, (3) $Ni_1Co_1Fe_1$-MOFs and (4) $Ni_1Co_1Fe_1$-MOFs + H_2O_2. Values are displayed as means ± s.d. ($n = 3$). *$P < 0.05$, **$P < 0.005$, ***$P < 0.001$. (**C**) Photographs of the bacterial colonies formed by *S. aureus* and *E. coli* in different treatment groups. (**D**) Fluorescence staining images of *S. aureus* and *E. coli* in different treatment groups. (**E**) SEM images of morphologies by *S. aureus* and *E. coli* in different treatment groups

cells of *S. aureus* and *E. coli* were observed to be severely damaged and almost completely destroyed, indicating that $Ni_1Co_1Fe_1$-MOFs combined with H_2O_2 performed more intensive antibacterial activity. Consequently, the established antibacterial system based on the Fenton-like reaction could inhibit *S. aureus* and *E. coli* effectively.

Intracellular ROS level detection

To further study the antibacterial mechanism of the established antibacterial system, $Ni_1Co_1Fe_1$-MOFs with a better antibacterial activity were chosen to evaluate the intracellular ROS level. As a cellular detection probe, DCFH-DA could be converted into cell membrane-impermeable DCFH by intracellular esterases, the non-fluorescent DCFH was then allowed to be oxidized into 2′,7′-dichlorodihydrofluorescein (DCF) with high fluorescence by intracellular ROS. Thus, DCFH-DA has been widely employed to determine the intracellular ROS level. As shown in Fig. 5A-B, compared with the control group, the ROS levels were slightly improved after treatment with H_2O_2 or $Ni_1Co_1Fe_1$-MOFs, while the cotreatment group caused much more prominent levels of intracellular ROS than the single treatment groups, indicating that the enhanced antibacterial activity was induced by the increased ROS catalyzed by $Ni_1Co_1Fe_1$-MOFs.

In vitro cytotoxicity assays

Biocompatibility was a primary requirement for the applications of $Ni_1Co_1Fe_1$-MOFs and $Ni_6Co_3Fe_1$-MOFs in medicine and food. Hence, after verifying the excellent antibacterial activities of the as-prepared MOFs, their cytotoxicity should be considered. Firstly, the effects of MOF concentration on the viability of 3T3 cells were examined (Fig. 5C-D). The results showed that both $Ni_1Co_1Fe_1$-MOFs and $Ni_6Co_3Fe_1$-MOFs exhibited ignorable cytotoxicity to 3T3 cells. The cell viability maintained greater than 90% in the concentration range of 12.5 to 100 μg/mL and decreased slightly only at the concentration of 200 μg/mL. Furthermore, at a low dose of H_2O_2, no obvious cytotoxicity was observed, and the viability of 3T3 cells remained at a high level after the addition of $Ni_1Co_1Fe_1$-MOFs or $Ni_6Co_3Fe_1$-MOFs. All the results demonstrated that the as-prepared $Ni_1Co_1Fe_1$-MOFs and $Ni_6Co_3Fe_1$-MOFs had excellent biocompatibility.

Fruit preservation study

Sodium alginate has the advantages of wide source, low cost, high safety, good film-forming ability, good biodegradability and biocompatibility [65]. In addition, the robust cross-linking property of sodium alginate colloids contributes to delaying weight loss by enhancing the barrier to moisture and oxygen, thus inhibiting the respiration and metabolism of the coated foods [66]. Therefore, sodium alginate was chosen as the fruit coating substrate in this study. Fruit storage trials were carried out to explore the utilization of biocompatible $Ni_1Co_1Fe_1$-MOF/sodium alginate composite coating for food preservation [67, 68]. The main purpose of constructing $Ni_1Co_1Fe_1$-MOF/sodium alginate coating was to add better antibacterial properties on the basis of the inherent barrier performance of sodium alginate. The polluted apple chunks were divided into three groups, including uncoated control, coated with $Ni_1Co_1Fe_1$-MOF/sodium alginate or $Ni_1Co_1Fe_1$-MOF/sodium alginate + H_2O_2. As shown in Fig. 5E, after storage for 10 d, the weight loss was significant in the uncoated apple chunks (5.98%), while the apple chunks coated with $Ni_1Co_1Fe_1$-MOF/sodium alginate showed much lower weight loss (1.01%), followed by those in the $Ni_1Co_1Fe_1$-MOF/sodium alginate + H_2O_2 (1.02%). Therefore, there was no need to compare with pure sodium alginate, and $Ni_1Co_1Fe_1$-MOF/sodium alginate coating still possessed barrier performance and delayed quality loss, no matter whether H_2O_2 was added or not. As shown in Fig. 5F, uncoated apple chunks showed almost no antibacterial effect, while the apple chunks coated with $Ni_1Co_1Fe_1$-MOF/sodium alginate or $Ni_1Co_1Fe_1$-MOF/sodium alginate + H_2O_2 effectively inhibited *E. coli* after storage for 2 d. Moreover, the $Ni_1Co_1Fe_1$-MOF/sodium alginate coating possessed better antibacterial performance after the addition of H_2O_2, which was ascribed to the Fenton-like catalytic reaction between $Ni_1Co_1Fe_1$-MOF and H_2O_2. These results revealed that $Ni_1Co_1Fe_1$-MOF/sodium alginate composite coating could significantly improve fruit storage by providing multiple preservation effects, such as delaying weightlessness and inhibiting bacteria. Thus, $Ni_1Co_1Fe_1$-MOF/sodium alginate composite coating could be promising for serving as an active agent in food antibacterial packaging.

Conclusions

In the current study, two kinds of trimetal-organic frameworks ($Ni_1Co_1Fe_1$-MOFs and $Ni_6Co_3Fe_1$-MOFs) with different atomic ratios of Ni/Co/Fe were successfully synthesized, which possessed excellent Fenton-like catalytic activity. Relative to M-MOFs (M = Ni, Co, Fe), both $Ni_1Co_1Fe_1$-MOFs and $Ni_6Co_3Fe_1$-MOFs presented more effective catalytic activities and $Ni_1Co_1Fe_1$-MOFs showed the highest catalytic efficiency, indicating that the introduction of Ni/Co/Fe effectively modified and improved the Fenton-like catalytic performance of NiCoFe-MOFs. In particular, $Ni_1Co_1Fe_1$-MOFs had stronger antibacterial properties than $Ni_6Co_3Fe_1$-MOFs because of the greater

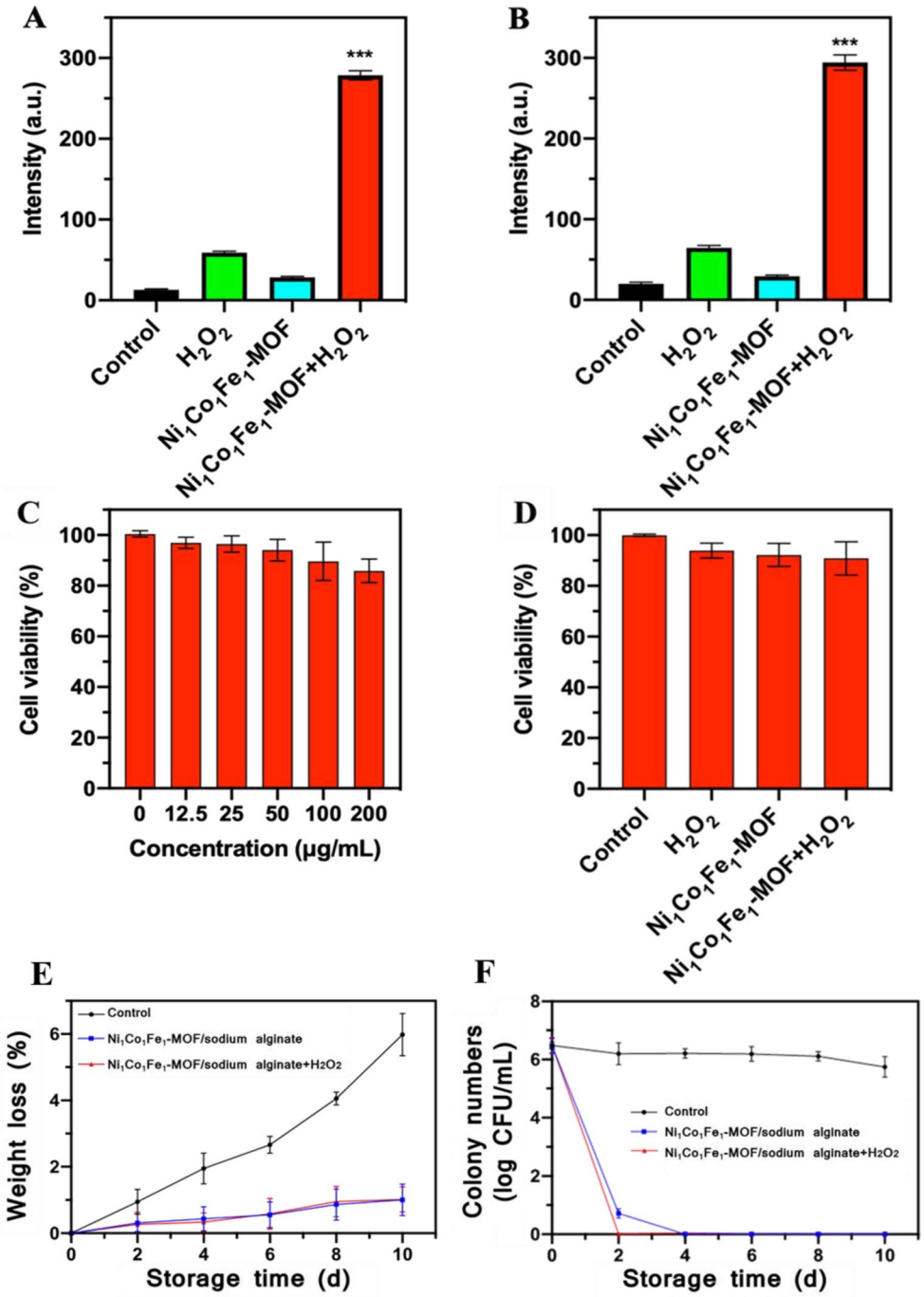

Fig. 5 Intracellular ROS levels of (**A**) *S. aureus* and (**B**) *E. coli* treated with (1) PBS, (2) H_2O_2, (3) $Ni_1Co_1Fe_1$-MOFs and (4) $Ni_1Co_1Fe_1$-MOFs + H_2O_2. Values are displayed as means ± s.d. ($n = 3$). $^*P < 0.05$, $^{**}P < 0.005$, $^{***}P < 0.001$. (**C**) Cell viability of 3T3 cells incubated with $Ni_1Co_1Fe_1$-MOFs at various concentrations (12.5, 25, 50, 100 and 200 μg/mL) for 24 h. (**D**) Cell viability of 3T3 cells incubated with different treatments: (1) PBS, (2) H_2O_2, (3) $Ni_1Co_1Fe_1$-MOFs and (4) $Ni_1Co_1Fe_1$-MOFs + H_2O_2. (**E**) Weight loss rates of apple chunks coated with PBS, $Ni_1Co_1Fe_1$-MOF/sodium alginate and $Ni_1Co_1Fe_1$-MOF/sodium alginate + H_2O_2. (**F**) Antibacterial effects of polluted apple chunks coated with PBS, $Ni_1Co_1Fe_1$-MOF/sodium alginate and $Ni_1Co_1Fe_1$-MOF/sodium alginate + H_2O_2

Fenton-like activity. Moreover, the fabricated antibacterial agent performed broad-spectrum antibacterial activities against both gram-positive (*S. aureus*) and gram-negative (*E. coli*) bacteria. In practice, NiCoFe-MOFs/sodium alginate complex coating provided multiple preservation effects for fruit storage. Above all, the constructed antibacterial system could be employed as a promising alternative to food antibacterial packaging.

Acknowledgements The authors are grateful to the Guangdong Basic and Applied Basic Research Foundation (2022A1515012489) for its support. This research was also supported by the International S&T Cooperation Projects of Guangdong Province (2022A0505050003), National Natural Science Foundation of China (3217161084) and the Common Technical Innovation Team of Guangdong Province on Preservation and Logistics of Agricultural Products (2023KJ145).

Funding Open Access funding provided by the IReL Consortium

Declarations

Conflict of interest All authors declare that they have no conflicts of interest.

References

1. W.Y. Zhang, J. Ma, D.-W. Sun, Raman spectroscopic techniques for detecting structure and quality of frozen foods: principles and applications. Critical Reviews in Food Science and Nutrition. **61**(16), 2623–2639 (2021). https://doi.org/10.1080/10408398.2020.1828814.
2. H. Jayan, D.-W. Sun, H.B. Pu, Q.Y. Wei, Surface-enhanced Raman spectroscopy combined with stable isotope probing to assess the metabolic activity of Escherichia coli cells in chicken carcass wash water. Spectrochimica Acta Part A: Molecular and Biomolecular Spectroscopy. **280**, 121549 (2022). https://doi.org/10.1016/j.saa.2022.121549.
3. Z.H. Wu, H.B. Pu, D.-W. Sun, Fingerprinting and tagging detection of mycotoxins in agri-food products by surface-enhanced Raman spectroscopy: principles and recent applications. Trends in Food Science & Technology. **110**, 393–404 (2021). https://doi.org/10.1016/j.tifs.2021.02.013.
4. Z.H. Wu, D.-W. Sun, H.B. Pu, Q.Y. Wei, A dual signal-on biosensor based on dual-gated locked mesoporous silica nanoparticles for the detection of Aflatoxin B1. Talanta. **253**, 124027 (2023). https://doi.org/10.1016/j.talanta.2022.124027.
5. H. Jayan, H.B. Pu, D.-W. Sun, Detection of bioactive metabolite in Escherichia coli culture using surface-enhanced Raman spectroscopy. Applied Spectroscopy. **76**(7), 812–822 (2022). https://doi.org/10.1177/00037028221079661.
6. Z.H. Wu, D.-W. Sun, H.B. Pu, Q.Y. Wei, A novel fluorescence biosensor based on CRISPR/Cas12a integrated MXenes for detecting Aflatoxin B1. Talanta **252**, 123773 (2023). https://doi.org/10.1016/j.talanta.2022.123773.
7. E.O. Asare, E.A. Mun, E. Marsili, V.N. Paunov, Nanotechnologies for control of pathogenic microbial biofilms. J. Mater. Chem. B **10**(27), 5129–5153 (2022). https://doi.org/10.1039/d2tb00233g.
8. X.Q. Tao, Z.Y. Liao, Y.Q. Zhang, F. Fu, M.Q. Hao, Y. Song, E.Q. Song, Aptamer-quantum dots and teicoplanin-gold nanoparticles constructed FRET sensor for sensitive detection of Staphylococcus aureus. Chin. Chem. Lett. **32**(2), 791–795 (2021). https://doi.org/10.1016/j.cclet.2020.07.020.
9. C.C. Hanna, Y.O. Hermant, P.W.R. Harris, M.A. Brimble, Discovery, synthesis, and optimization of peptide-based antibiotics. Acc. Chem. Res. **54**(8), 1878–1890 (2021). https://doi.org/10.1021/acs.accounts.0c00841.
10. Z.W. Chen, X.B. Liao, Y. Yang, L. Han, Z.X. He, Y.Y. Dong, K.F.H. Yeo, X.B. Sun, T.X. Xue, Y.F. Xie, W.D. Wang, Analysis of rainwater storage and use recommendations: from the perspective of DBPs generation and their risks. J. Hazard. Mater. **448**, 130833 (2023). https://doi.org/10.1016/j.jhazmat.2023.130833.
11. H. Jayan, H.B. Pu, D.-W. Sun, Recent developments in Raman spectral analysis of microbial single cells: techniques and applications. Critical Reviews in Food Science and Nutrition. **62**(16), 4294–4308 (2021). https://doi.org/10.1080/10408398.2021.1945534.
12. D.R. Zhang, L.J. Huang, D.-W. Sun, H.B. Pu, Q.Y. Wei, Bio-interface engineering of MXene nanosheets with immobilized lysozyme for light-enhanced enzymatic inactivation of methicillin-resistant Staphylococcus aureus. Chemical Engineering Journal. **452**(2), 139078 (2023). https://doi.org/10.1016/j.cej.2022.139078.
13. Z.H. Wu, D.-W. Sun, H.B. Pu, Q.Y. Wei, X.R. Lin, Ti3C2Tx MXenes loaded with Au nanoparticle dimers as a surface-enhanced Raman scattering aptasensor for AFB1 detection. Food Chemistry. **372**, 131293 (2022). https://doi.org/10.1016/j.foodchem.2021.131293.
14. H. Jayan, D.-W. Sun, H.B. Pu, Q.Y. Wei, Mesoporous silica coated core-shell nanoparticles substrate for size-selective SERS detection of chloramphenicol. Spectrochimica Acta Part A: Molecular and Biomolecular Spectroscopy. **284**, 121817 (2023). https://doi.org/10.1016/j.saa.2022.121817.
15. H.Y. He, D.-W. Sun, Z.H. Wu, H.B. Pu, Q.Y. Wei, On-off-on fluorescent nanosensing: materials, detection strategies and recent food applications. Trends in Food Science & Technology. **119**, 243–256 (2022). https://doi.org/10.1016/j.tifs.2021.11.029.
16. H.Y. He, D.-W. Sun, H.B. Pu, Z.H. Wu, A SERS-fluorescence dual-signal aptasensor for sensitive and robust determination of AFB1 in nut samples based on Apt-Cy5 and MNP@Ag-PEI. Talanta. **253**, 123962 (2023). https://doi.org/10.1016/j.talanta.2022.123962.
17. S. Kali, M. Khan, M.S. Ghaffar, S. Rasheed, A. Waseem, M.M. Iqbal, M.B.K. Niazi, M.I. Zafar, Occurrence, influencing factors, toxicity, regulations, and abatement approaches for disinfection by-products in chlorinated drinking water: a comprehensive review. Environ. Pollut. **281**, 116950 (2021). https://doi.org/10.1016/j.envpol.2021.116950.
18. M.J. Li, L. Nan, C.Y. Liang, Z.Q. Sun, L. Yang, K. Yang, Antibacterial behavior and related mechanisms of martensitic Cu-bearing stainless steel evaluated by a mixed infection model of C Escherichia coli and Staphylococcus aureus in vitro. J. Mater. Sci. Technol. **62**, 139–147 (2021). https://doi.org/10.1016/j.jmst.2020.05.030.
19. M.M. Khan, S.N. Matussin, A. Rahman, Recent development of metal oxides and chalcogenides as antimicrobial agents. Bioprocess Biosyst. Eng. **46**(9), 1231–1249 (2023). https://doi.org/10.1007/s00449-023-02878-1.
20. Y.H. Yan, Y.Z. Li, Z.W. Zhang, X.H. Wang, Y.Z. Niu, S.H. Zhang, W.L. Xu, C.G. Ren, Advances of peptides for antibacterial applications. Collolds Surf. B: Biointerfaces. **202**, 111682 (2021). https://doi.org/10.1016/j.colsurfb.2021.111682.
21. Z. Sadat, F. Farrokhi-Hajiabad, F. Lalebeigi, N. Naderi, M.G. Gorab, R.A. Cohan, R. Eivazzadeh-Keihan, A. Maleki, A comprehensive review on the applications of carbon-based nanostructures in wound healing: from antibacterial aspects to cell growth stimulation. Biomaterials Sci. **10**(24), 6911–6938 (2022). https://doi.org/10.1039/d2bm01308h.
22. L. Xu, Z. Zhu, D.-W. Sun, Bioinspired nanomodification strategies: moving from chemical-based agrosystems to sustainable agriculture. ACS Nano. **15**(8), 12655–12686 (2021). https://doi.org/10.1021/acsnano.1c03948.
23. L.J. Huang, D.-W. Sun, Z.H. Wu, H.B. Pu, Q.Y. Wei, Reproducible, shelf-stable, and bioaffinity SERS nanotags inspired by multivariate polyphenolic chemistry for bacterial identification. Analytica Chimica Acta. **1167**, 338570 (2021). https://doi.org/10.1016/j.aca.2021.338570.
24. L.J. Sun, L.M. Li, Q. Fu, X.R. Qian, Monitoring buried flap in pharyngeal defect reconstruction. Cellulose. **30**(6), 3569–3588 (2023). https://doi.org/10.1007/s10570-023-05106-x.

25. Y. Yuan, H. Wu, H.F. Lu, Y.R. Zheng, J.Y. Ying, Y.G. Zhang, ZIF nano-dagger coated gauze for antibiotic-free wound dressing. Chem. Commun. **55**(5), 699–702 (2019). https://doi.org/10.1039/c8cc08568d.
26. L. Jiao, J.Y.R. Seow, W.S. Skinner, Z.U. Wang, H.-L. Jiang, Metal–organic frameworks: structures and functional applications. Mater. Today. **27**, 43–68 (2019). https://doi.org/10.1016/j.mattod.2018.10.038.
27. L.L. Wu, H.B. Pu, L.J. Huang, D.-W. Sun, Plasmonic nanoparticles on metal-organic framework: a versatile SERS platform for adsorptive detection of new coccine and orange II dyes in food. Food Chem. **328**, 127105 (2020a). https://doi.org/10.1016/j.foodchem.2020.127105.
28. M.C. Lv, D.-W. Sun, L.J. Huang, H.B. Pu, Precision release systems of food bioactive compounds based on metal-organic frameworks: synthesis, mechanisms and recent applications. Critical Reviews in Food Science and Nutrition. **62**(15), 3991–4009(2022). https://doi.org/10.1080/10408398.2021.2004086.
29. H.B. Pu, H.F. Zhu, F. Xu, D.-W. Sun, Development of core-satellite-shell structured MNP@Au@MIL-100(Fe) substrates for surface enhanced Raman spectroscopy and their applications in trace level determination of malachite green in prawn. Journal of Raman Spectroscopy. **53**(4), 682–693(2022). https://doi.org/10.1002/jrs.6293.
30. D.-W. Sun, L.J. Huang, H.B. Pu, J. Ma, Introducing reticular chemistry into agrochemistry. Chemical Society Reviews. **50**(2), 1070–1110(2021). https://doi.org/10.1039/c9cs00829b.
31. Q.Z. Qian, Y.P. Li, Y. Liu, L. Yu, G.Q. Zhang, Ambient fast synthesis and active sites deciphering of hierarchical foam-like trimetal-organic framework nanostructures as a platform for highly efficient oxygen evolution electrocatalysis. Adv. Mater. **31**(23), 1901139 (2019). https://doi.org/10.1002/adma.201901139.
32. B. Mohan, A. Kamboj, K. Virender, Singh, G. Priyanka, Singh, A.J.L. Pombeiro, P. Ren, Metal-organic frameworks (MOFs) materials for pesticides, heavy metals, and drugs removal: environmental safety. Sep. Purif. Technol. **310**, 123175 (2023). https://doi.org/10.1016/j.seppur.2023.123175.
33. Z.H. Lin, Z.Y. Yuan, K.F. Wang, X.Z. He, Synergistic tuning mixed matrix membranes by Ag^{+}-doping in UiO-66-NH_2/polymers of intrinsic microporosity for remarkable CO_2/N_2 separation. J. Membr. Sci. **681**, 121775 (2023). https://doi.org/10.1016/j.memsci.2023.121775.
34. H.M. Ren, B.Y. Liu, B.T. Zuo, Z.F. Li, G. Li, The effect of free carboxylic acid groups on the proton conductivity of a series of UiO-66-Ce(IV) metal-organic frameworks. Microporous Mesoporous Mater. **351**, 112481 (2023). https://doi.org/10.1016/j.micromeso.2023.112481.
35. Y.M. Jo, Y.K. Jo, J.H. Lee, H.W. Jang, I.S. Hwang, D. Yoo, MOF-based chemiresistive gas sensors: toward new functionalities. Adv. Mater. **35**(43), 2206842 (2023). https://doi.org/10.1002/adma.202206842.
36. M. Oggianu, N. Monni, V. Mameli, C. Cannas, S.A. Sahadevan, M.L. Mercuri, Designing magnetic nanoMOFs for biomedicine: current trends and applications. Magnetochemistry. **6**(3), 39 (2020). https://doi.org/10.3390/magnetochemistry6030039.
37. M.Y. Lan, X.W. Zhang, H.Y. Chu, C.C. Wang, MIL-101(fe) and its composites for catalytic removal of pollutants: synthesis strategies, performances and mechanisms. Progress Chem. **35**(3), 458–474 (2023). https://doi.org/10.7536/PC220822.
38. L.J. Huang, D.-W. Sun, H.B. Pu, C.Y. Zhang, D.R. Zhang, Nanocellulose-based polymeric nanozyme as bioinspired spray coating for fruit preservation. Food Hydrocolloids. **135**, 108138 (2023). https://doi.org/10.1016/j.foodhyd.2022.108138.
39. L.J. Huang, D.-W. Sun, H.B. Pu, Photosensitized peroxidase mimicry at the hierarchical 0D/2D heterojunction-like quasi metal-organic framework interface for boosting biocatalytic disinfection. Small. **18**(20), 2200178 (2022). https://doi.org/10.1002/smll.202200178.
40. G. Wyszogrodzka, B. Marszalek, B. Gil, P. Dorozynski, Metal-organic frameworks: mechanisms of antibacterial action and potential applications. Drug Discovery Today. **21**(6), 1009–1018 (2016). https://doi.org/10.1016/j.drudis.2016.04.009.
41. Y.S. Raval, D. Fleming, A. Mohamed, M.J. Karau, J.N. Mandrekar, A.N. Schuetz, K.E. Greenwood-Quaintance, H. Beyenal, R. Patel, In vivo activity of hydrogen-peroxide generating electrochemical bandage against murine wound infections. Adv. Ther. **6**(5), 2300059 (2023). https://doi.org/10.1002/adtp.202300059.
42. Y. Li, W.S. Ma, J. Sun, M. Lin, Y.S. Niu, X.C. Yang, Y.H. Xu, Electrochemical generation of Fe_3C/N-doped graphitic carbon nanozyme for efficient wound healing in vivo. Carbon. **159**, 149–160 (2020). https://doi.org/10.1016/j.carbon.2019.11.093.
43. Y.X. Wang, C.X. Zhang, H. Zhang, L.H. Feng, L.B. Liu, A hybrid nano-assembly with synergistically promoting photothermal and catalytic radical activity for antibacterial therapy. Chin. Chem. Lett. **33**(10), 4605–4609 (2022). https://doi.org/10.1016/j.cclet.2022.03.076.
44. M. Zouanti, M. Bezzina, R. Dhib, Experimental study of degradation and biodegradability of oxytetracycline antibiotic in aqueous solution using Fenton process. Environ. Eng. Res. **25**(3), 316–323 (2020). https://doi.org/10.4491/eer.2018.343.
45. D.T. Yue, X. Yan, C. Guo, X.F. Qian, Y.X. Zhao, NiFe layered double hydroxide (LDH) nanosheet catalysts with Fe as electron transfer mediator for enhanced persulfate activation. J. Phys. Chem. Lett. **11**(3), 968–973 (2020). https://doi.org/10.1021/acs.jpclett.9b03597.
46. S.T. Gao, Y. Jin, K. Ge, Z.H. Li, H.F. Liu, X.Y. Dai, Y.H. Zhang, S.Z. Chen, X.J. Liang, J.C. Zhang, Self-supply of O_2 and H_2O_2 by a nanocatalytic medicine to enhance combined chemo/chemodynamic therapy. Adv. Sci. **6**(24), 1902137 (2019). https://doi.org/10.1002/advs.201902137.
47. L. Zhang, Y. Dai, S. Pan, Y. Tan, C. Sun, M. Cao, H. Xu, Copper-selenocysteine quantum dots for NIR-II photothermally enhanced chemodynamic therapy. ACS Appl. Bio Mater. **5**(4), 1794–1803 (2022). https://doi.org/10.1021/acsabm.2c00150.
48. L.S. Lin, J.B. Song, L. Song, K.M. Ke, Y.J. Liu, Z.J. Zhou, Z.Y. Shen, J. Li, Z. Yang, W. Tang, G. Niu, H.H. Yang, X.Y. Chen, Simultaneous Fenton-like ion delivery and glutathione depletion by MnO_2-based nanoagent to enhance chemodynamic therapy. Angew. Chem. **57**(18), 4902–4906 (2018). https://doi.org/10.1002/anie.201712027.
49. D.Z. Yang, Z.Z. Chen, Z. Gao, S.K. Tammina, Y.L. Yang, Nanozymes used for antimicrobials and their applications. Colloids Surf., B **195**, 111252 (2020). https://doi.org/10.1016/j.colsurfb.2020.111252.
50. Q.S. Wu, H.P. Yang, L. Kang, Z. Gao, F.F. Ren, Fe-based metal-organic frameworks as Fenton-like catalysts for highly efficient degradation of tetracycline hydrochloride over a wide pH range: acceleration of Fe(II)/Fe(III) cycle under visible light irradiation. Appl. Catal. B **263**, 118282 (2020b). https://doi.org/10.1016/j.apcatb.2019.118282.
51. M.L. Chen, T.H. Lu, L.L. Long, Z. Xu, L. Ding, Y.H. Cheng, NH_2-Fe-MILs for effective adsorption and Fenton-like degradation of imidacloprid: removal performance and mechanism investigation. Environ. Eng. Res. **27**(2), 200702 (2022). https://doi.org/10.4491/eer.2020.702.
52. Z.M. Feng, J.W. Yang, L.Y. Zhu, T. Sun, Bromine functionalized Fe/Cu bimetallic MOFs for accelerating Fe(III)/Fe (II) cycle and efficient degradation of phenol in Fenton-like system. Colloids Surf., a **658**, 130701 (2023). https://doi.org/10.1016/j.colsurfa.2022.130701.
53. D.M. Li, Z.W. Zhu, D.-W. Sun, Visualization and quantification of content and hydrogen bonding state of water in apple and

potato cells by confocal Raman microscopy: a comparison study. Food Chemistry. **385**, 132679 (2022). https://doi.org/10.1016/j.foodchem.2022.132679.
54. D.M. Li, Z.W. Zhu, D.-W. Sun, Quantification of hydrogen bonding strength of water in saccharide aqueous solutions by confocal Raman microscopy. Journal of Molecular Liquids. **342**,117498 (2021). https://doi.org/10.1016/j.molliq.2021.117498.
55. C.Y. Lin, X.J. Guo, L.X. Chen, T.H. You, J. Lu, D.P. Sun, Ultrathin trimetallic metal-organic framework nanosheets for accelerating bacteria-infected wound healing. J. Colloid Interface Sci. **628**, 731–744 (2022). https://doi.org/10.1016/j.jcis.2022.08.073.
56. X. Han, X.B. Yang, G.B. Liu, Z.H. Li, L. Shao, Boosting visible light photocatalytic activity via impregnation-induced RhB-sensitized MIL-125(Ti). Chem. Eng. Res. Des. **143**, 90–99 (2019). https://doi.org/10.1016/j.cherd.2019.01.010.
57. C.Y. Zhang, L.J. Huang, H.B. Pu, D.-W. Sun, Magnetic surface-enhanced Raman scattering (MagSERS) biosensors for microbial food safety: fundamentals and applications. Trends in Food Science & Technology. **113**, 366–381 (2021). https://doi.org/10.1016/j.tifs.2021.05.007.
58. N. Hussain, H.B. Pu, D.-W. Sun, Synthesis of bimetallic core-shelled nanoparticles modified by 2-mercaptoethanol as SERS substrates for detecting ferbam and thiabendazole in apple puree. Food Additives & Contaminants: Part A: Chemistry, Analysis, Control, Exposure & Risk Assessment. **38**(8), 1386–1399 (2021). https://doi.org/10.1080/19440049.2021.1933207.
59. H. Jayan, H.B. Pu, D.-W. Sun, Analyzing macromolecular composition of E. Coli O157:H7 using Raman-stable isotope probing. Spectrochimica Acta Part A: Molecular and Biomolecular Spectroscopy. **276**, 121217 (2022). https://doi.org/10.1016/j.saa.2022.121217.
60. Q. Sun, M. Liu, K.Y. Li, Y.T. Han, Y. Zuo, F.F. Chai, C.S. Song, G.L. Zhang, X.W. Guo, Synthesis of Fe/M(M = Mn, Co, Ni) bimetallic metal organic frameworks and their catalytic activity for phenol degradation under mild conditions. Inorg. Chem. Front. **4**(1), 144–153 (2017). https://doi.org/10.1039/c6qi00441e.
61. C. Xu, R. Fang, L. Chen, Y. Li, Functional metal–organic frameworks for catalytic applications. Coord. Chem. Rev. **388**, 268–292 (2019).
62. M. Wang, J.L. Xia, J.C. Jiang, S.H. Li, K. Huang, W. Mao, M. Li, A novel liquid Ca/Zn thermal stabilizer synthesized from Tung-maleic anhydride and its effects on thermal stability and mechanical properties of PVC. Polym. Degrad. Stab. **133**, 136–143 (2016). https://doi.org/10.1016/j.polymdegradstab.2016.08.010.
63. Y. Sun, Z.X. Yang, P.F. Tian, Y.Y. Sheng, J. Xu, Y.F. Han, Oxidative degradation of nitrobenzene by a Fenton-like reaction with Fe-Cu bimetallic catalysts. Appl. Catal. B **244**, 1–10 (2019). https://doi.org/10.1016/j.apcatb.2018.11.009.
64. X. Fan, F. Yang, J.B. Huang, Y. Yang, C.X. Nie, W.F. Zhao, L. Ma, C. Cheng, C.S. Zhao, R. Haag, Metal-organic-framework-derived 2D carbon nanosheets for localized multiple bacterial eradication and augmented anti-infective therapy. Nano Lett. **19**(9), 5885–5896 (2019). https://doi.org/10.1021/acs.nanolett.9b01400.
65. D.R. Zhang, H.B. Pu, L.J. Huang, D.-W. Sun, Advances in flexible surface-enhanced Raman scattering (SERS) substrates for nondestructive food detection: fundamentals and recent applications. Trends in Food Science & Technology. **109**,690–701 (2021). https://doi.org/10.1016/j.tifs.2021.01.058.
66. M. Smyth, M.S. M'Bengue, M. Terrien, C. Picart, J. Bras, E.J. Foster, The effect of hydration on the material and mechanical properties of cellulose nanocrystal-alginate composites. Carbohydr. Polym. **179**, 186–195 (2018). https://doi.org/10.1016/j.carbpol.2017.09.002.
67. W.Y. Zhang, D.-W. Sun, J. Ma, J.H. Cheng, Z.M. Wang, B.Z. Tang, A volatile basic nitrogens-responsive tag based on aggregation-induced emission luminogen for real-time monitoring and in situ visualization of salmon freshness. Analytica Chimica Acta. **1221**, 340122 (2022). https://doi.org/10.1016/j.aca.2022.340122.
68. Y. Liu, H.B. Pu, Q. Li, D.-W. Sun, Discrimination of pericarpium citri reticulatae in different years using terahertz time-domain spectroscopy combined with convolutional neural network. Spectrochimica Acta Part A: Molecular and Biomolecular Spectroscopy. **286**, 122035 (2023). https://doi.org/10.1016/j.saa.2022.122035.